The 2.7-Å crystal structure of a 194-kDa homodimeric fragment of the 6-deoxyerythronolide B synthase

Yinyan Tang*†, Chu-Young Kim*†‡, Irimpan I. Mathews†§, David E. Cane¶, and Chaitan Khosla*‖

*Departments of Chemistry and Chemical Engineering, Stanford University, Stanford, CA 94305; §Stanford Synchrotron Radiation Laboratory, 2575 Sand Hill Road, Menlo Park, CA 94025; and ¶Department of Chemistry, Brown University, Providence, RI 02912

Edited by JoAnne Stubbe, Massachusetts Institute of Technology, Cambridge, MA, and approved June 7, 2006 (received for review March 9, 2006)

The x-ray crystal structure of a 194-kDa fragment from module 5 of the 6-deoxyerythronolide B synthase has been solved at 2.7 Å resolution. Each subunit of the homodimeric protein contains a full-length ketosynthase (KS) and acyl transferase (AT) domain as well as three flanking "linkers." The linkers are structurally well defined and contribute extensively to intersubunit or interdomain interactions, frequently by means of multiple highly conserved residues. The crystal structure also reveals that the active site residue Cys-199 of the KS domain is separated from the active site residue Ser-642 of the AT domain by ≈80 Å. This distance is too large to be covered simply by alternative positioning of a statically anchored, fully extended phosphopantetheine arm of the acyl carrier protein domain from module 5. Thus, substantial domain reorganization appears necessary for the acyl carrier protein to interact successively with both the AT and the KS domains of this prototypical polyketide synthase module. The 2.7-Å KS–AT structure is fully consistent with a recently reported lower resolution, 4.5-Å model of fatty acid synthase stucture, and emphasizes the close biochemical and structural similarity between polyketide synthase and fatty acid synthase enzymology.

modular megasynthase | multienzyme assembly | polyketide synthase

Modular polyketide synthases (PKSs), such as the 6-deoxyerythronolide B synthase (DEBS), are a large family of polyfunctional, multisubunit enzymes that catalyze the biosynthesis of structurally complex and medicinally important natural products (1, 2). Similar to vertebrate fatty acid synthases (FASs) (3), each PKS module consists of at least two catalytic domains [a ketosynthase (KS) and an acyl transferase (AT)] that together collaborate with an acyl carrier protein (ACP) domain to catalyze polyketide chain elongation and intermodular chain transfer (Fig. 1). In most modules, additional domains such as ketoreductase (KR), dehydratase, and enoylreductase catalyze further modification of the initial β-ketoacylthioester product of KS-catalyzed chain elongation.

As illustrated in Fig. 6, which is published as supporting information on the PNAS web site, the primary amino acid sequences of individual PKS modules are characterized by stretches of highly conserved regions (corresponding to the above-mentioned domains) flanked by 20–300 residue "linkers" that lack homology to each other or to other protein families in sequence databases (4, 5). With the exception of C-terminal/N-terminal linker pairs (6) that serve as docking sites for successive but noncovalently interacting modules, the structure and function of linkers in modular PKSs have been largely unexplored. There is growing appreciation, however, that a better understanding of the role of linkers is of critical importance to the continued success of biosynthetic engineering (6–8).

Very recently, we have been able to dissect a PKS module into individual active KS–AT and ACP components that together can be reconstituted to restore all of the normal catalytic properties of an intact homodimeric module (9). We have now solved the 2.7-Å crystal structure of a 194-kDa homodimeric fragment containing the KS–AT didomain of DEBS module 5. The crystallized fragment contains the full-length KS and AT domains as well as three flanking peptide linkers: the N-terminal linker, an intervening KS–to–AT domain or KS–to–AT linker, and a peptide linker C-terminal to the AT domain that includes the first 30 residues of the AT-to-KR interdomain region of module 5 previously deduced solely on the basis of sequence alignments. In addition to providing an atomic-level insight into the structure and topological organization of the core catalytic domains of a multimodular PKS, this prototypical structure also complements and extends a recently reported lower resolution, a 4.5-Å model of type I fatty acid synthase structure. The results provide a perspective for future biochemical and engineering investigations into this remarkable family of modular megasynthases.

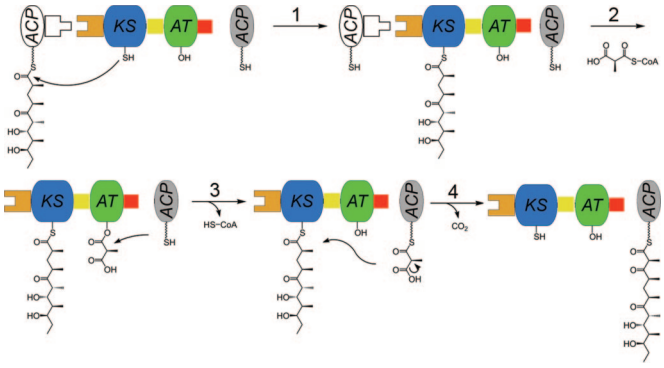

Fig. 1. Chain elongation cycle catalyzed by a minimal PKS module. In this example, the crystallized KS–AT fragment is shown in color, whereas the ACP domains that interact with the KS and AT are in black and white or grayscale. (1) A methylmalonyl unit that is added to a pentaketide substrate to yield the hexaketide product. KS is primed with a growing polyketide chain by the upstream ACP. AT is acylated with a methylmalonyl extender unit from its CoA derivative (2), which is transferred to the downstream ACP (3) and condensation takes place in the active site of KS with the release of carbon dioxide (4). The extended polyketide chain is anchored on the downstream ACP. Domains are drawn in the order they appear in amino acid sequence of the module. Orange, N-terminal docking domain; blue, ketosynthase (KS); green, acyl transferase (AT); gray, acyl carrier protein (ACP); yellow, the KS–to–AT linker; red, post-AT linker peptide. The phosphopantetheine prosthetic group of the ACP is drawn as a curly line. The same coloring scheme is used in subsequent figures.

Conflict of interest statement: No conflicts declared.

This paper was submitted directly (Track II) to the PNAS office.

Abbreviations: ACP, acyl carrier protein; AT, acyl transferase; DEBS, 6-deoxyerthronolide B synthase; FAS, fatty acid synthase; KR, ketoreductase; KS, ketosynthase; PKS, polyketide synthase.

Data deposition: The atomic coordinates have been deposited in the Protein Data Bank, www.pdb.org (PDB ID code 2HG4).

†Y.T., C.-Y.K., and I.I.M. contributed equally to this work.

‡Present address: Department of Biological Sciences, National University of Singapore, 14 Science Drive 4, Singapore 117543.

‖To whom correspondence should be addressed. E-mail: khosla@stanford.edu.

Table 1. Summary of crystallographic analysis

Data sets	Remote (λ1)	Inflection (λ2)	Peak (λ3)
Crystallographic statistics			
Wavelength, Å	0.9392	0.9793	0.9789
Resolution, Å	48–2.7	49–2.8	48–3.0
Unique reflections	206,652	181,814	152,290
Completeness, % (outer shell)	99.8 (99.9)	99.8 (99.9)	99.0 (98.7)
R_{sym}* (outer shell)	0.112 (0.68)	0.103 (0.57)	0.127 (0.55)
Data redundancy (outer shell)	3.8 (3.8)	3.8 (3.8)	7.6 (7.6)
Average I/s (outer shell)	8.1 (1.9)	9.4 (2.3)	11.8 (4.1)
Mean figure of Meirt (30–2.9 Å)		0.49	
Refinement statistics			
Resolution range, Å	48–2.7		
No. of reflections ($F > 0$)	196,207		
Total no. of atoms (water)	39,402 (310)		
Completeness of data, %	99.8		
R-factor† (R-free)	0.216 (0.255)		
rms deviation‡			
Bond, Å	0.013		
Angle, °	1.46		
Ramachandran plot			
Most favored, %	87.3		
Additionally allowed, %	11.9		
Generously allowed, %	0.6		
Disallowed, %	0.2		

*$R_{sym} = \Sigma_h\Sigma_i |I_{h,i} - I_h| / \Sigma_h\Sigma_i I_{h,i}$, where I_h is the mean intensity of the i observations of symmetry-related reflections of h.

†$R = \Sigma|F_{obs} - F_{calc}|/\Sigma F_{obs}$, where $F_{obs} = F_P$, and F_{calc} is the calculated protein structure factor from the atomic model (R_{free} was calculated with 5% of the reflections).

‡rms deviation in bond lengths and angles are the deviations from ideal values.

Results and Discussion

The structure of the crystallized fragment of DEBS module 5, which was solved by multiwavelength anomalous dispersion (MAD), has 40,908 atoms (582 kDa) per asymmetric unit (Table 1). To our knowledge, this structure is the x-ray crystal structure with the largest number of atoms per asymmetric unit that has been solved to date by using the MAD technique.

Overall Organization. Each monomer of this homodimeric 194-kDa protein contains one KS domain, one AT domain, and three structurally well defined linker regions (Fig. 2), each with a unique secondary structure: the helical linker at the N terminus of the KS domain, the KS–to–AT linker between the KS and AT domains, and the linker at the C terminus of each AT domain. Although the 194-kDa KS–AT fragment is considerably smaller than the intact 314-kDa DEBS module 5 that harbors an additional KR domain and an ACP domain, several naturally occurring minimal PKS modules [e.g., module 6 from the narbonolide synthase (10), module 2 from the rifamycin synthase (11), and module 14 from the rapamycin synthase (12)] consist almost entirely of a KS–AT homologue of the crystallized fragment plus an attached ACP domain. Given the ≈10-kDa size of a typical ACP domain, the x-ray structure described here provides insights into the architecture of 95% of a minimal PKS module.

The 2,828-Å^2 dimer interface of the KS–AT fragment of DEBS module 5 lies along the 2-fold axis of the homodimer and is composed of two distinct regions: the interface between the two KS domains of the homodimer and the coiled-coil structure of the N-terminal peptide dimer. Each KS domain adopts an $\alpha\beta\alpha\beta\alpha$ fold, similar to the homologous condensing enzymes of type II fatty acid synthases (13–15) and type II polyketide synthases (16, 17). Superposition of the Cα atoms of the KS domain and the *Escherichia coli* β-ketoacyl-acyl carrier protein synthase I (13) yields an rms deviation of 1.36 Å for 332 Cα atoms. The KS dimer interface is anchored around two antiparallel β-strands (residues 192–196 from each subunit) interacting with each other through backbone hydrogen bonds. Additionally, there are two salt bridges at the interface between Glu-160 and Arg-157 side chains of the paired subunits. The lack of conservation of this pair of charged residues among PKS modules presumably contributes to the specificity for homodimeric

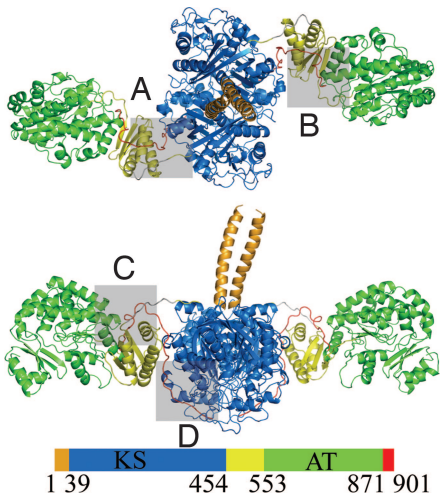

Fig. 2. X-ray crystal structure of the KS–AT didomain from DEBS module5. The KS–AT protein forms a homodimer. Orange, N-terminal coiled coil linker domain; blue, ketosynthase (KS) domain; green, acyl transferase (AT) domain; yellow, KS–to–AT linker; red, post-AT linker peptide. Residues 458–465, which lack electron density, are manually modeled and shown in gray. Interdomain interactions detailed in Fig. 4 (*vide infra*) are highlighted in gray boxes. (*A* and *B*) Top view. (*C* and *D*) Side view.

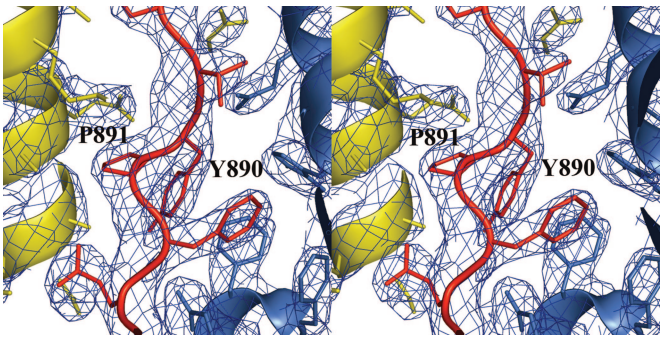

Fig. 3. Electron density map of the post-AT linker peptide. The $2F_o - F_c$ map is contoured at 1.5 σ.

association of subunits in a bacterial cell that coexpresses one or more multimodular PKSs.

The dimeric N-terminal peptides (Fig. 2) have a coiled-coil structure consistent with the results of earlier mutant complementation and NMR structural studies (6, 18–21). These N-terminal linkers have been shown to play an important role in mediating intermodular polyketide chain transfer by providing a docking site for a compatible linker attached to the C terminus of the ACP domain of the upstream module (6, 18–21). The helices of this coiled coil protrude outward from the KS dimer to the solvent and do not make contact with rest of the protein, providing free access for interaction with the C-terminal linker region of the upstream module. The coiled-coil interface is formed by the hydrophobic residues Leu-12, Leu-16, Thr-19, Leu-23, Val-26, Thr-27, and Leu-30, as well as a salt bridge between Arg29A and Glu34B at the base of the coiled coil. As with the KS dimer interface, these side chains are not conserved and presumably enable the specificity of homodimerization of PKS modules.

The AT domain (Fig. 2) contains an α,β-hydrolase-like core domain and an appended smaller subdomain with a ferredoxin-like structure. The architecture of the AT domain is similar to that of the *E. coli* and the *Streptomyces coelicolor* malonyl-CoA:ACP transacylases (22, 23) (rms deviation of 1.59 Å and 1.49 Å, respectively, for 242 and 223 Cα atom superposition). A notable difference is the C-terminal helix (residues 857–867) of the DEBS module 5 AT domain, which interacts closely with the KS–to–AT linker (see the following three paragraphs).

A second, well-structured linker domain (residues 455 to 552) is found between the KS and AT domains of each subunit of the 194-kDa fragment (Fig. 2). This KS–to–AT linker domain is formed by a three-stranded β-sheet packed against two α-helices on one side and represents a protein fold not previously reported in the Protein Data Bank. The C-terminal helix of the AT domain stacks on the other side of the three-stranded β-sheet of the KS–to–AT linker domain, resulting in an $\alpha\beta\alpha$ fold for this domain.

Finally, the 30-aa peptide appended to the C terminus of the AT domain wraps back over both the AT domain and the KS–to–AT linker so as to interact specifically with the KS domain (Fig. 2 *C* and *D*). Although the specific length of the linker peptide immediately downstream of the AT domain varies from module to module, depending on the domains that follow (ACP, dehydratase, enoylreductase, or KR), the residues in the 30-aa C-terminal peptide linker that are observed in the KS–AT crystal structure are well conserved, with good electron density (Fig. 3), indicating that they are well-ordered in the crystal.

Both the KS–to–AT linker and the C-terminal post-AT linker peptide play important structural roles in fixing the relative positions of the KS and AT domains. In particular, two highly conserved hydrophobic cores at the KS:KS–to–AT linker interface and the KS–to–AT linker:AT interface highlight the architectural significance of these regions. The interface between the KS domain and the KS–to–AT linker (Fig. 4*A*) includes residues from both the KS domain (Phe-98, Phe-102, Phe-103, Ile-105, Ala-110, Leu-121, Trp-125, Pro-135, and Leu-186) and the KS–to–AT linker (Trp-513), as well as the C-terminal post-AT linker peptide (Tyr-890 and Phe-892). Similarly, interface between the KS–to–AT linker and the AT domain (Fig. 4*B*) includes residues from both the AT domain (Trp-628, His-631, Phe-859, His-860, Leu-863, Gly-864, and Tyr-867) and the KS–to–AT linker (Pro-469, Val-471, Phe-504, Ala-507, Val-518, and Ala-543), as well as the post-AT linker peptide (Val-873, Trp-875, and Phe-879). Each of the above sets of hydrophobic residues, which are highly conserved in type I (modular) PKSs (Fig. 6) but not in type II (dissociated) synthases, presumably play a role in organizing the relative positioning of the PKS domains. Additional interactions between individual domains and linkers are established through specific hydrogen bonds. For example, the AT domain and the KS–to–AT linker interact through hydrogen bonds between Arg-516 and Tyr-867 (carbonyl oxygen) as well as between Arg-541 and Asp-858 (side chain OD2) (Fig. 4*C*). Similarly, the post-AT linker peptide forms eight hydrogen bonds with the KS domain and five hydrogen bonds with the KS–to–AT linker (Fig. 4*D*). Interestingly, these hydrogen bonds use exclusively main chain backbone atoms, a structural feature that could facilitate the construction of domain-swapped hybrid modules. In summary, the KS domain, the KS–to–AT linker, the AT domain, and the post-AT linker peptide are packed together in an apparently rigid arrangement that precludes significant movement of the KS and AT domains relative to one another.

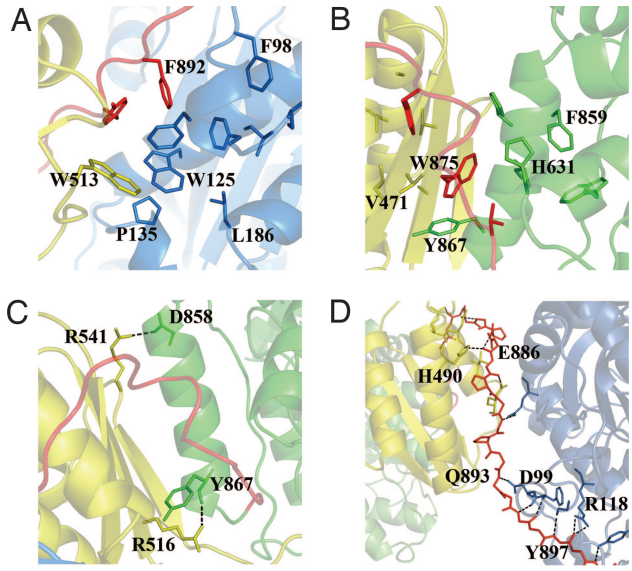

Fig. 4. Protein–protein interactions in the KS–AT didomain (for clarity, only selected residues are labeled). Locations of the interacting regions are shown in Fig. 2. (*A*) Highly conserved hydrophobic core at the interface between the KS domain, the KS–to–AT linker, and the post-AT linker peptide. (*B*) Highly conserved hydrophobic core at the interface between the AT domain, the KS–to–AT linker, and the post-AT linker peptide. (*C*) Two key hydrogen bonds between the AT domain and the KS–to–AT linker. (*D*) Hydrogen bonds between the KS domain, the KS–to–AT linker, and the post-AT linker peptide.

Active Sites of the KS and AT Domains. Analogous to type II fatty acid and polyketide ketosynthases (13–17), the active site of the dimeric KS of DEBS module 5 is buried and extends toward the dimer interface (Fig. 5*A*). An extended substrate-binding pocket in each KS domain is centered around the active site cysteine

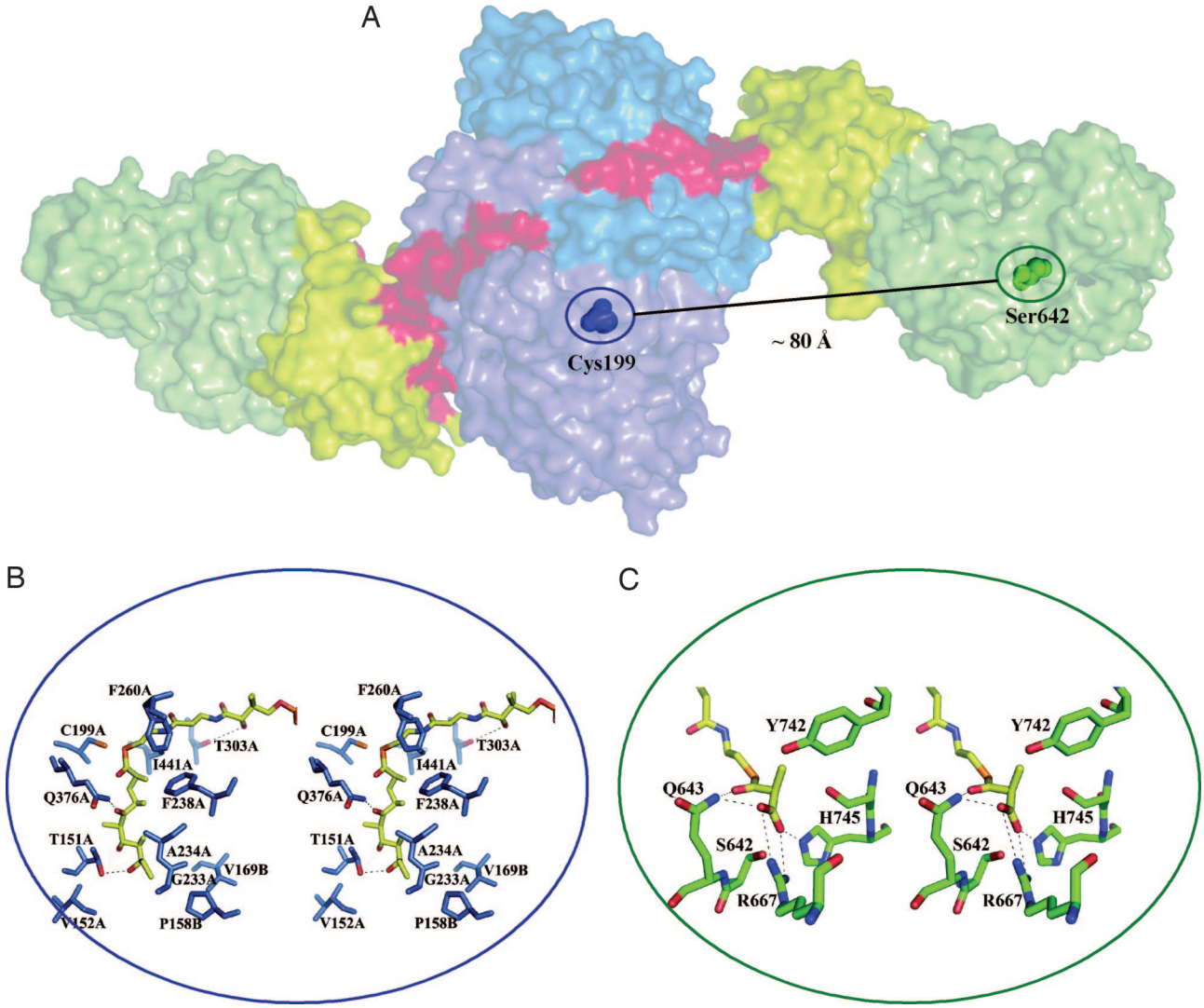

Fig. 5. Proposed substrate binding sites of the KS and AT domains. (*A*) The surfaces of the individual KS domains are shown in blue and purple. The KS active site is separated from the AT active site by ≈80 Å. (*B*) Model of the pentaketide-phosphopantetheine group in the KS active site near the KS:KS dimer interface. (*C*) Model of the (2*S*)-methylmalonyl-phosphopantetheine group in the active site of the AT domain.

residue (Cys-199) (Fig. 5*A*). Structural comparison of the active sites of the substrate-bound (24) and uncomplexed (14) ketosynthase II from the *E. coli* fatty acid synthase has previously identified two residues, Ile-108 and Phe-400 (*E. coli* KS numbering), that undergo ligand-induced conformational changes on substrate binding (13). In the homodimeric KS of DEBS module 5, these two residues are replaced by smaller side chains, Thr-151 and Ile-441, respectively. These smaller side chains allow the KS5 dimer to adopt a conformation corresponding to the previously reported substrate-bound state of the *E. coli* FAS KS, thereby allowing us to model the natural phosphopantetheinyl-linked pentaketide substrate into the KS substrate-binding channel (Fig. 5*B*). According to this model, the ketone carbonyl oxygen at C-5 of the pentaketide is hydrogen-bonded to the side chain amide nitrogen of Gln-376, whereas the C-9 OH is hydrogen-bonded to Thr-151. The ethyl group at the end of the pentaketide chain is predicted to bind at the dimer interface in a hydrophobic pocket formed by Val152A, Gly233A, Ala234A, Pro158B, and Val169B. The attached phosphopantetheine group would be held in place by a hydrogen bond to Thr-303 and hydrophobic interactions with Phe-238, Phe-260, and Ile-441 in the substrate-binding pocket.

The extensive domain-linker interactions within DEBS module 5 result in significant structural changes at the KS active site relative to homologues from type II PKSs. In particular, the interactions between residues 892–901 of the post-AT linker peptide and the KS domain lead to substantial conformational differences between the two classes of active sites. For example, a conserved helix at the KS dimer interface of type II enzymes is replaced with a loop corresponding to residues 153–161 in module 5. This change contributes to a larger substrate-binding cavity, consistent with earlier observations that DEBS KS5 can accommodate substrate analogues such as a decaketide that are longer than the natural pentaketide substrate (25).

A bound acetate anion was found near the active site Ser-642 residue of the AT domain in the structure of the KS–AT homodimer. This acetate anion facilitated modeling of a methylmalonyl-phosphopantetheine substrate into the AT active site (Fig. 5*C*). A 20-Å deep channel, which lies between the two subdomains of the AT, is lined by highly conserved residues. In this model, the invariant Arg-667 at the base of this binding pocket forms a salt bridge with the α-carboxylate of the methylmalonyl-CoA substrate. The methylmalonyl binding pocket of the module 5 AT domain is considerably larger than the malonyl

binding pocket of the homologous *S. coelicolor* malonyl-CoA:ACP transacylase (22).

The AT domains play a crucial role as gatekeepers in polyketide biosynthesis. Given their ability to discriminate between malonyl and methylmalonyl polyketide chain extension units, their substrate specificity has been extensively investigated (26–28). The previously proposed role of Tyr-742 and Gln-643 in controlling specificity for (2*S*)-methylmalonyl-CoA (27, 28) is clarified by the x-ray structure of the KS–AT homodimer (Fig. 5*C*). In addition to the predicted hydrophobic interaction of Tyr-742 with the α-methyl group of the substrate, Gln 643 can orient the bound methylmalonyl through a hydrogen bond with the substrate carboxylate. By contrast, the side chain of His-745 would cause a steric clash with the methyl group of (2*R*)-methylmalonyl-CoA, thereby accounting for the observed stereochemical specificity (Fig. 5*C*).

Interaction Between the ACP Domain and the KS–AT Fragment: Not Just a Swinging Arm. The classical model for vertebrate fatty acid synthases and modular polyketide synthases assumes that a statically anchored ACP domain reaches the active sites of the KS, AT, and reductive domains through its 18-Å long and flexible phosphopantetheine arm (29). Unexpectedly, the crystal structure of the 194-kDa KS–AT didomain argues against such a simplistic picture of multifunctional PKS catalysis. The crystal structure reveals that the Cys-199 in the active site of the KS domain is separated by ≈80 Å from the active site residue Ser-642 of the nearest AT domain (Fig. 5). This distance is too large to be covered simply by alternative positioning of a fixed, fully extended phosphopantetheine arm. Thus, substantial domain reorganization is necessary for the ACP domain and its covalently tethered substrates to interact successively with first the AT and then the KS domain of the paired subunit of the DEBS module. Similar requirements for major conformational changes have been predicted in other multienzyme systems (30, 31). How the requisite quaternary structural changes that accompany catalysis are achieved remains unknown at present and is the subject of ongoing investigations into the structure and mechanism of modular PKS megasynthases.

Comparision to the Vertebrate Fatty Acid Synthases. The domain architecture and enzymology of modular PKSs and vertebrate FASs are closely related. While this manuscript was in preparation, Maier *et al.* (32) reported the 4.5-Å crystal structure of the porcine fatty acid synthase. The quaternary structure was deduced by modeling homologous template structures of individual subunits from bacterial FASs into the observed electron density of the vertebrate FAS, guided by the visible secondary structural elements. The overall topology of the KS-malonyl acyltransferase portion of the deduced FAS structure is strikingly similar to the higher resolution 2.7-Å crystal structure of the KS–AT fragment of DEBS module 5 reported here (Fig. 7, which is published as supporting information on the PNAS web site). In both systems, the KS domains form a homodimer centered around the 2-fold rotational axis, although each of the monomeric AT domains are located at opposite sides of the KS dimer, with a 70- to 80-Å distance between the KS and AT active sites. Whereas the extensive intervening peptide regions flanking the KS, AT, and other domains of the porcine FAS are undefined in the 4.5-Å crystal structure, the atomic resolution structure of the DEBS KS–AT homodimer allows precise definition of the structure of the three peptide linkers that flank the KS and AT domains. The N-terminal peptide linker seen in the DEBS protein lacks a counterpart in the FAS sequence or structure, presumably because it has evolved to facilitate the directional transfer of growing polyketide chains between successive modules of a multimodular PKS. In contrast, the observed $\alpha\beta\alpha$ fold of the KS–to–AT linker fits well into the corresponding unresolved electron density of the FAS homodimer. Similarly, the orientation of the post-AT linker peptide in the DEBS KS–AT homodimer allows it to span the distance between the assigned malonyl acyltransferase and dehydratase domains of the porcine FAS. Although sequence alignments of the latter two linker regions reveal very limited identity between the FAS and PKS proteins, both the hydrophobic residues (discussed in *Overall Organization*) involved in domain-domain interactions as well as the structurally constrained proline residues in the post-AT linker peptide of DEBS module 5 are conserved among vertebrate FAS sequences (Fig. 6). We also note that the recently reported structure of a DEBS KR domain (33), and the proposed model of the β-carbon processing dehydratase, KR, and enoylreductase domains, is fully consistent with the upper arms containing the homologous reductive domains of the low resolution FAS structure and indicates how the structure of the minimal PKS module, represented by the KS–AT didomain, can be expanded to include additional domains without fundamental reorganization of the core KS–AT topology (Fig. 7). Together, these observations highlight the ancient evolutionary relationships between modular PKSs and vertebrate FASs, and set the stage for systematic dissection of the biochemical roles of these conserved architectural motifs. They also open the door to approaches to the structure-based design of antibiotics through rational biosynthetic engineering of modular megasynthases.

Materials and Methods

Cloning, Expression, and Purification of the 194-kDa Homodimeric KS–AT Fragment of DEBS Module 5. Plasmid pAYC10 encoding the KS–AT didomain from DEBS module 5 was constructed as follows: A fragment from the natural BsiWI site to the Tyr-Gln junction site was amplified by using primers 5′-GCGAGGCG-TACGCGCAGGGCGTGGAGGTCG-3′ and 5′-ACCTGG-TAGCGCCAGTCGTCGTCCTCGT-3′ and cloned into pCR-BluntII-TOPO. The resulting intermediate plasmid was digested with BsiWI and EcoRI and cloned into the corresponding restriction sites in pRSG46 containing pET21 expression vector to yield pAYC10 (6). Transformed *E. coli* BL21 (DE3) cells were grown in LB medium at 37°C until an OD_{600} of 0.6 before the cultures were cooled to 18°C, induced with 0.2 mM isopropyl-β-D-galactopyranoside, and grown for an additional 14 h at 18°C. Cells were harvested by centrifugation (4,420 × *g* for 15 min), resuspended in lysis/wash buffer [50 mM phosphate (pH 7.6), 300 mM NaCl, and 10 mM imidazole], and lysed by sonication (5 × 1 min). After centrifugation, cellular debris was removed, and nickel-NTA agarose resin (Qiagen) was added directly to the supernatant (1 ml of resin per 1 L of cells). The protein was allowed to bind to the resin in batch form for 20 min at 4°C, and the slurry was poured into a fritted column, washed with 10-column volumes of lysis/wash buffer, and eluted with 3-column volumes of elution buffer (50 mM phosphate, 100 mM NaCl, and 150 mM imidazole). The eluate was applied directly to a Hi-TrapQ anion exchange column (Amersham Pharmacia) and eluted with an increasing linear gradient of NaCl. KS–AT eluted at ≈370 mM NaCl. The purified protein was buffer exchanged into 20 mM Hepes at pH 7.6 and concentrated to 3 mg/ml. Selenomethionine-labeled protein was expressed in BL21 (DE3) cells by using the method of Van Duyne *et al.* (34) and purified as described.

Crystallization and Data Collection for 194-kDa Homodimeric KS–AT Fragment of DEBS Module 5. Crystals were grown at room temperature by using the hanging-drop vapor-diffusion method. The well buffer contained 0.1 M Tris (pH 8.5), 0.2 M Li_2SO_4, and 30% PEG4000. The crystals belong to the space group C2 and contain six monomers per symmetric unit. The unit cell has

dimensions of a = 305.3 Å, b = 150.1 Å, c = 184.4 Å, and β = 110°. Crystals from the selenomethionine (SeMet)-labeled protein was used for the structure solution. Because of the crystal decay in the radiation, multiple wavelength data for several crystals were collected at the Stanford Synchrotron Radiation Laboratory (SSRL) beamlines. Two data sets, inflection and remote wavelength from one crystal and the peak wavelength from a second crystal, were used for the structure solution were collected at beamline 11–1. The data sets were collected at 100 K and processed by using HKL2000 (35) and XDS (36) software packages.

Structure Determination 194-kDa Homodimeric KS–AT Fragment of DEBS Module 5. The structure was solved by multiwavelength anomalous dispersion phasing. At 4.7 Å resolution, 85 selenium (Se) sites were found by using the program SHELXD (37). Further phase improvement by using SHARP (38) enabled the location of 90 Se sites. The electron density maps were improved by 6-fold averaging (there are six monomers in the asymmetric unit) by using the RESOLVE (39) program. The automated tracing procedure implemented in RESOLVE traced ≈3,000 residues. Maps were examined by using the program O (40) and were determined to be of good quality. Similar quality maps were also generated by performing histogram matching, solvent flattening, and 6-fold NCS averaging by using the program DM (41). Extensive manual building by using maps generated from RESOLVE, SHARP, and DM enabled the complete tracing of a single monomer. The hexamer was then generated by using the NCS operators. The atomic model was refined by using REFMAC (42). The final model contains 5,281 residues, 6 acetate ions, 5 sulfate ions, 5 chlorine atoms, and 310 water molecules. Residues 1–8, 412–414, and 458–465 are absent from the final model because of the lack of interpretable electron density in the corresponding regions. The statistics for the final model are in Table 1. Atomic coordinates of the KS–AT homodimer have been deposited in the Protein Data Bank (PDB ID code 2HG4).

Molecular Docking. For the docking of the substrate, the coordinates of phosphopantetheinyl-linked pentaketide and (2*S*)-methylmalonyl-phosphopantetheinyl substrate were obtained from the Dundee PRODRG server (43). The coordinates were read into O (40) and manually docked in the active-site. The molecular coordinates of the docked complex were energy minimized in CNS (44).

This work was supported by National Institutes of Health Grants CA 66736 (to C.K.) and GM 22172 (to D.E.C.). Portions of this research were carried out at the Stanford Synchrotron Radiation Laboratory, a national user facility operated by Stanford University on behalf of the U.S. Department of Energy Office of Basic Energy Sciences.

1. Walsh, C. T. (2004) *Science* **303,** 1805–1810.
2. Cane, D. E., Walsh, C. T. & Khosla, C. (1998) *Science* **282,** 63–68.
3. Asturias, F. J., Chadick, J. Z., Cheung, I. K., Stark, H., Witkowski, A., Joshi, A. K. & Smith, S. (2005) *Nat. Struct. Mol. Biol.* **12,** 225–232.
4. Cortes, J., Haydock, S. F., Roberts, G. A., Bevitt, D. J. & Leadlay, P. F. (1990) *Nature* **348,** 176–178.
5. Donadio, S., Staver, M. J., McAlpine, J. B., Swanson, S. J. & Katz, L. (1991) *Science* **252,** 675–679.
6. Gokhale, R. S., Tsuji, S. Y., Cane, D. E. & Khosla, C. (1999) *Science* **284,** 482–485.
7. Ranganathan, A., Timoney, M., Bycroft, M., Cortes, J., Thomas, I. P., Wilkinson, B., Kellenberger, L., Hanefeld, U., Galloway, I. S., Staunton, J. & Leadlay, P. F. (1999) *Chem. Biol.* **6,** 731–741.
8. Hans, M., Hornung, A., Dziarnowski, A., Cane, D. E. & Khosla, C. (2003) *J. Am. Chem. Soc.* **125,** 5366–5374.
9. Chen, A. Y., Schnarr, N. A., Kim, C. Y., Cane, D. E. & Khosla, C. (2006) *J. Am. Chem. Soc.* **128,** 3067–3074.
10. Xue, Y., Zhao, L., Liu, H. W. & Sherman, D. H. (1998) *Proc. Natl. Acad. Sci. USA* **95,** 12111–12116.
11. August, P. R., Tang, L., Yoon, Y. J., Ning, S., Muller, R., Yu, T. W., Taylor, M., Hoffmann, D., Kim, C. G., Zhang, X., *et al.* (1998) *Chem. Biol.* **5,** 69–79.
12. Schwecke, T., Aparicio, J. F., Molnar, I., Konig, A., Khaw, L. E., Haydock, S. F., Oliynyk, M., Caffrey, P., Cortes, J., Lester, J. B., *et al.* (1995) *Proc. Natl. Acad. Sci. USA* **92,** 7839–7843.
13. Olsen, J. G., Kadziola, A., von Wettstein-Knowles, P., Siggaard-Andersen, M., Lindquist, Y. & Larsen, S. (1999) *FEBS Lett.* **460,** 46–52.
14. Huang, W., Jia, J., Edwards, P., Dehesh, K., Schneider, G. & Lindqvist, Y. (1998) *EMBO J.* **17,** 1183–1191.
15. Davies, C., Heath, R. J., White, S. W. & Rock, C. O. (2000) *Structure (London)* **8,** 185–195.
16. Pan, H., Tsai, S., Meadows, E. S., Miercke, L. J., Keatinge-Clay, A. T., O'Connell, J., Khosla, C. & Stroud, R. M. (2002) *Structure (London)* **10,** 1559–1568.
17. Keatinge-Clay, A. T., Maltby, D. A., Medzihradszky, K. F., Khosla, C. & Stroud, R. M. (2004) *Nat. Struct. Mol. Biol.* **11,** 888–893.
18. Tsuji, S. Y., Wu, N. & Khosla, C. (2001) *Biochemistry* **40,** 2317–2325.
19. Tsuji, S. Y., Cane, D. E. & Khosla, C. (2001) *Biochemistry* **40,** 2326–2331.
20. Kumar, P., Li, Q., Cane, D. E. & Khosla, C. (2003) *J. Am. Chem. Soc.* **125,** 4097–4102.
21. Broadhurst, R. W., Nietlispach, D., Wheatcroft, M. P., Leadlay, P. F. & Weissman, K. J. (2003) *Chem. Biol.* **10,** 723–731.
22. Keatinge-Clay, A. T., Shelat, A. A., Savage, D. F., Tsai, S. C., Miercke, L. J., O'Connell, J. D., III, Khosla, C. & Stroud, R. M. (2003) *Structure (London)* **11,** 147–154.
23. Serre, L., Verbree, E. C., Dauter, Z., Stuitje, A. R. & Derewenda, Z. S. (1995) *J. Biol. Chem.* **270,** 12961–12964.
24. Moche, M., Schneider, G., Edwards, P., Dehesh, K. & Lindqvist, Y. (1999) *J. Biol. Chem.* **274,** 6031–6034.
25. Hunziker, D. Wu., N., Kenoshita, K., Cane, D. E. & Khosla, C. (1999) *Tetrahedron Lett.* **40,** 635–638.
26. Lau, J., Cane, D. E. & Khosla, C. (2000) *Biochemistry* **39,** 10514–10520.
27. Haydock, S. F., Aparicio, J. F., Molnar, I., Schwecke, T., Khaw, L. E., Konig, A., Marsden, A. F., Galloway, I. S., Staunton, J. & Leadlay, P. F. (1995) *FEBS Lett.* **374,** 246–248.
28. Reeves, C. D., Murli, S., Ashley, G. W., Piagentini, M., Hutchinson, C. R. & McDaniel, R. (2001) *Biochemistry* **40,** 15464–15470.
29. Chirala, S. S., Jayakumar, A., Gu, Z. W. & Wakil, S. J. (2001) *Proc. Natl. Acad. Sci. USA* **98,** 3104–3108.
30. Evans, J. C., Huddler, D. P., Hilgers, M. T., Romanchuk, G., Matthews, R. G. & Ludwig, M. L. (2004) *Proc. Natl. Acad. Sci. USA* **101,** 3729–3736.
31. Milne, J. L., Shi, D., Rosenthal, P. B., Sunshine, J. S., Domingo, G. J., Wu, X., Brooks, B. R., Perham, R. N., Henderson, R. & Subramaniam, S. (2002) *EMBO J.* **21,** 5587–5598.
32. Maier, T., Jenni, S. & Ban, N. (2006) *Science* **311,** 1258–1263.
33. Keatinge-Clay, A. T., Stroud, R. M. (2006) *Structure (London)* **14,** 737–748.
34. Van Duyne, G. D., Standaert, R. F., Karplus, P. A., Schreiber, S. L. & Clardy, J. (1993) *J. Mol. Biol.* **229,** 105–124.
35. Otwinowski, Z. & Minor, W. (1997) *Methods Enzymol.* **276,** 307–326.
36. Kabsch, W. (1993) *J. Appl. Cryst.* **26,** 795–800.
37. Schneider, T. R. S., G. M. (2002) *Acta Crystallogr. D* **58,** 1772–1779.
38. de La Fortelle, E. & Bricogne, G. (1997) *Methods Enzymol.* **276,** 472–494.
39. Terwilliger, T. C. (2003) *Acta Crystallogr. D* **59,** 38–44.
40. Jones, T. A., Zou, J. Y., Cowan, S. W. & Kjeldgaard, M. (1991) *Acta Crystallogr. A* **47,** 110–119.
41. Cowtan, K. (1994) *Joint CCP4 and ESF-EACBM Newsletter of Protein Crystallography* **31,** 34–38.
42. Murshudov, G. N., Vagin, A. A. & Dodson, E. J. (1997) *Acta Crystallogr. D* **53,** 240–255.
43. Schuettelkopf, A. V. & Aalten, D. M. F. v. (2004) *Acta Crystallogr. D* **60,** 1355–1363.
44. Brunger, A. T., Adams, P. D., Clore, G. M., DeLano, W. L., Gros, P., Grosse-Kunstleve, R. W., Jiang, J. S., Kuszewski, J., Nilges, M., Pannu, N. S., *et al.* (1998) *Acta Crystallogr. D* **54,** 905–921.